23. J. Okabayashi *et al.*, *Phys. Rev. B*, in press.
24. S. von Molnár, H. Munekata, H. Ohno, L. L. Chang, *J. Magn. Magn. Mater.* **93**, 356 (1991).
25. Y. Satoh, N. Inoue, Y. Nishikawa, J. Yoshino, *3rd Symposium on Physics and Application of Spin-Related Phenomena in Semiconductors*, Sendai, Japan, 17 to 18 November 1997, H. Ohno, Y. Oka, J. Yoshino, Eds., pp. 23–25.
26. T. Story, R. R. Galazka, R. B. Frankel, P. A. Wolff, *Phys. Rev. Lett.* **56**, 777 (1986).
27. H. Ohno *et al.*, *Appl. Phys. Lett.* **73**, 363 (1998).
28. B. Heinrich and J. A. C. Bland, Eds., *Ultrathin Magnetic Structures* (Springer-Verlag, Berlin, 1994), vol. 2, chap. 2, and references therein.
29. N. Akiba *et al.*, unpublished data.
30. S. Tarucha *et al.*, *Phys. Rev. Lett.* **77**, 3613 (1996).
31. D. Goldhaber-Gordon *et al.*, *Nature* **391**, 156 (1998).
32. S. F. Alvarado, *Phys. Rev. Lett.* **75**, 513 (1995).
33. D. J. Monsma, R. Vlutters, J. C. Lodder, *Science* **281**, 407 (1998).
34. J. M. Kikkawa and D. D. Awschalom, *Phys. Rev. Lett.* **80**, 4313 (1998).
35. S. Koshihara *et al.*, *ibid.* **78**, 4617 (1997).
36. I acknowledge F. Matsukura, A. Shen, N. Akiba, Y. Sugawara, T. Kuroiwa, T. Omiya, Y. Iye, S. Katsumoto, A. Oiwa, and T. Dietl for collaboration and discussion. Partially supported by a Grant-in-Aid for Scientific Research Priority Area "Spin Controlled Semiconductor Nanostructures" (09244103) from the Ministry of Education, Science, Sports and Culture, Japan, and by the "Research for the Future" program (JSPS-RFTF97P00202) from the Japan Society for the Promotion of Science.

The Roles of Structural Imperfections in InGaN-Based Blue Light–Emitting Diodes and Laser Diodes

Shuji Nakamura

REVIEW

High-efficiency light-emitting diodes emitting amber, green, blue, and ultraviolet light have been obtained through the use of an InGaN active layer instead of a GaN active layer. The localized energy states caused by In composition fluctuation in the InGaN active layer are related to the high efficiency of the InGaN-based emitting devices. The blue and green InGaN quantum-well structure light-emitting diodes with luminous efficiencies of 5 and 30 lumens per watt, respectively, can be made despite the large number of threading dislocations (1×10^8 to 1×10^{12} cm^{-2}). Epitaxially laterally overgrown GaN on sapphire reduces the number of threading dislocations originating from the interface of the GaN epilayer with the sapphire substrate. InGaN multi-quantum-well structure laser diodes formed on the GaN layer above the SiO_2 mask area can have a lifetime of more than 10,000 hours. Dislocations increase the threshold current density of the laser diodes.

The brightness and durability of light-emitting diodes (LEDs) make them ideal for displays, and semiconductor laser diodes (LDs) have been used in numerous device applications from optical communications systems to compact disk (CD) players. These applications have been limited, however, by the lack of materials that can emit blue light efficiently. Full-color displays, for example, require at least three primary colors, usually red, green, and blue, to produce any visible color. Such a combination is also needed to make a white light–emitting device that would be more durable and consume less power than conventional incandescent bulbs or fluorescent lamps. The shorter wavelength means that the light can be focused more sharply, which would increase the storage capacity of magnetic and optical disks. Digital versatile disks (DVDs), which came onto the market in 1996, rely on red aluminum indium gallium phosphide (AlInGaP) semiconductor lasers and have a data capacity of about 4.7 gigabytes (Gbytes), compared to 0.65 Gbytes for compact disks. By moving to violet wavelengths emitted by III-V nitride-based semiconductors, the capacity could be increased to 15 Gbytes. The violet III-V nitride-based LDs could also improve the performance of laser printers and undersea optical communications. Such III-V nitride-based semiconductors have a direct band gap that is suitable for blue light–emitting devices. The band gap energy of aluminum gallium indium nitride (AlGaInN) varies between 6.2 and 2.0 eV, depending on its composition, at room temperature (RT). Thus, by using these semiconductors, red- to ultraviolet (UV)-emitting devices can be fabricated.

The first breakthrough for III-V nitride-based semiconductors was the use of AlN (*1*, *2*) or GaN (*3*, *4*) nucleation layers for the GaN growth. By using these nucleation layers, it became possible to obtain high-quality GaN films with a mirrorlike flat surface, a low residual carrier concentration, high carrier mobilities, and a strong photoluminescence (PL) intensity. The second big breakthrough for III-V nitride-based LEDs and LDs was that *p*-type GaN was obtained, and the reasons why *p*-type GaN had not been obtained were clarified. For the LEDs and LDs, a *p*-*n* junction is used to inject carriers (holes and electrons) into the active layers from *p*-type layer and *n*-type layer. Thus, control of both *p*-type and *n*-type conductivity is required to fabricate those devices. It was relatively easy to make *n*-type GaN from the beginning. However, it was virtually impossible to obtain *p*-type GaN films for many years (*5*, *6*). The unavailability of *p*-type GaN films had prevented III-V nitrides from being used in light-emitting devices, such as blue LEDs and LDs. Since the 1970s, many people had tried to make *p*-type GaN by doping with Zn (*7*), Be (*8*), Mg (*9*), Cd (*10*), and similar metals as an acceptor impurity. However, unknown reasons prevented the formation of a low-resistivity, *p*-type GaN by doping.

In 1989, Amano *et al.* (*11*) obtained *p*-type GaN films by using Mg-doping as an acceptor impurity and a post low-energy electron-beam irradiation (LEEBI) treatment by means of metal organic chemical vapor deposition (MOCVD) growth method. After the growth, LEEBI treatment was performed for Mg-doped GaN films to obtain a low-resistivity *p*-type GaN film. The LEEBI treatment was thought to displace Mg through the energy of the electron beam irradiation. In spite of this achievement in forming *p*-type GaN, only Amano *et al*. had succeeded in obtaining *p*-type GaN until 1992 because the mechanism of the LEEBI treatment was not understood exactly. In 1992, Nakamura *et al*. (*12*, *13*) obtained *p*-type GaN films by thermal annealing of GaN films in a N_2-ambient instead of the LEEBI treatment. Before thermal annealing, the resistivity of Mg-doped GaN films was $\sim 1 \times 10^6$ ohm·cm. After thermal annealing at temperatures above 700°C, the resistivity dropped to 2 ohm·cm (*12*). Low-resistivity *p*-type GaN films, which were obtained by N_2-ambient thermal annealing, showed a resistivity as high as 1×10^6 ohm·cm after NH_3-ambient thermal annealing at temperatures above 600°C (*13*).They proposed that atomic hydrogen produced by NH_3 dissociation at temperatures above 400°C was related to the acceptor com-

The author is in the Department of Research and Development, Nichia Chemical Industries, 491 Oka, Kaminaka, Anan, Tokushima 774, Japan. E-mail: shuji@nichia.co.jp

pensation mechanism (*13*). A hydrogenation process whereby acceptor-H neutral complexes were formed in *p*-type GaN films was proposed (*13*). The formation of acceptor-H neutral complexes causes acceptor compensation. This hydrogenation process has been accepted as the acceptor compensation mechanism of *p*-type III-V nitride-based semiconductor by many researchers (*14–18*). Theoretical calculations of this hydrogen passivation were made by Neugebauer and Van De Walle (*18*). Thus, in 1992, the 20-year mystery of *p*-type GaN was resolved.

The third big breakthrough was that high-quality InGaN films have become available. As mentioned above, an InGaN active layer is used for all of the III-V nitride-based LEDs and LDs to emit red to UV light. Thus, InGaN is the most important compound semiconductor among III-V nitride compounds because the InGaN active layer emits light by the recombination of the injected electrons and holes into the InGaN. In spite of its importance, no one had succeeded in obtaining high-quality InGaN films that could emit a strong band-to-band emission at RT by optical pumping or current injection (*19–21*). In 1992, Nakamura and Mukai (*22*) succeeded in growing high-quality InGaN films that emitted strong band-to-band emission from green to UV by changing the In content of InGaN with a two-flow MOCVD method. Finally, Nakamura *et al.* (*23*) grew a InGaN multi-quantum-well (MQW) structure and confirmed an enhanced strong PL intensity from quantized energy levels in a InGaN well layer with a thickness of 25 Å. Adding a small amount of In into the GaN is very important to obtain a strong band-to-band emission at RT. The reason is related to the presence of deep localized energy states (*24–28*).

In 1994, Nakamura *et al*. developed blue InGaN/AlGaN double heterostructure LEDs (*29*) and then developed blue/green InGaN single quantum-well (SQW) structure LEDs in 1995 (*30*). Then, UV/amber LEDs (*31*, *32*) and RT violet laser light emission in InGaN/GaN/AlGaN–based heterostructures under pulsed operations were achieved (*33*). Since Nakamura *et al.*'s report of pulsed operation, many groups have reported pulsed operation of the LDs using the same structure (*34–40*). The latest results showed that the lifetime can be as long as 1000 (*41*) and 10,000 hours (*42*) under RT continuous-wave (CW) operation. Also, high-power LDs were fabricated using epitaxially lateral overgrown GaN (ELOG) (*43*) and GaN substrates (*44*). All of these light-emitting devices use an InGaN active layer instead of a GaN active layer because it is difficult to fabricate a highly efficient light-emitting device using a GaN active layer, for reasons not yet understood. Also, the InGaN active layer in these LEDs and LDs include a large number of threading dislocations (TDs), from 1×10^8 to 1×10^{12} cm^{-2}, that originate from the interface between GaN and the sapphire substrate due to a large lattice mismatch of 15% (*24*, *45*). The TDs are thought to form as a result of a complex set of interactions that include the interface energy, the nucleation density, and island coalescence (*46*). In spite of this large number of dislocations, the efficiency of the InGaN-based LEDs and LDs is much greater than that of the conventional III-V compound semiconductor (AlGaAs and AlInGaP)-based LEDs and LDs. In many conventional optoelectronic devices, the device performance has been limited by the control of both point defects and structural defects in these materials. However, these recent reports now suggest that III-V nitride–based devices are less sensitive to dislocations than conventional III-V semiconductors.

Numerous studies have investigated the origin of these defects (*47*) and their effects on the structural (*48*), optical (*49*, *50*), electronic (*51*, *52*), and morphological (*46*, *53–55*) properties of heteroepitaxial GaN layers. Dislocations have been associated with the deep-level yellow luminescence band centered at 2.2 to 2.4 eV (*56*). Recently, it was confirmed that these TDs affect device performance. The TDs served as a diffusion pathway of metals and acted as a leakage current pathway in InGaN and GaN (*57*, *58*). For InGaN layer, an open hexagonal inverted pyramid called "V-defect" (*59*), spatial inhomogeneities of In composition (*60*, *61*), and pit formations (*62*, *63*) initiated at TDs in GaN film were reported. In particular, many studies of the spatial inhomogeneities of In composition in InGaN have been performed (*24–28*).

Lester *et al*. (*45*) observed high TD density ($>2 \times 10^{10}$ cm^{-2}) in the film of high-efficient InGaN/AlGaN–based blue LEDs (*3*, *29*) and concluded that in nitride materials TDs are not efficient recombination sites, under the assumption that minority carrier diffusion lengths are comparable to those of other III-V materials. Through this work, it was suggested that the diffusion lengths could be substantially smaller than those of conventional III-V materials. Rosner *et al*. (*50*) characterized the correlation between TDs as observed by transmission electron microscopy (TEM), surface morphology as observed by atomic force microscopy (AFM), and wavelength-resolved cathodoluminescence (CL) imaging. The pits observed in the surface of GaN films grown on C-face sapphire were the termination of TDs. The dark areas in the CL images were regions of the film where minority carriers were depleted due to high nonradiative recombination velocity at these dislocations. Then, they suggested that a diffusion length of minority carrier (hole) was not greater than 250 nm. Sugahara *et al.* (*64*) observed the TD at the same location of *n*-type GaN films using plan-view TEM and CL images to study the TDs. There was a clear one-to-one correspondence between the dark spots observed in CL images and the dislocations in TEM images, indicating that the dislocations are nonradiative recombination centers. The minority carrier (hole) diffusion length was estimated to be ~50 nm by the analysis of the CL dark spots. It was concluded that the efficiency of light emission is high as long as the minority carrier diffusion length is shorter than the dislocation spacing. For example, if the minority carrier diffusion length is 50 nm, the dislocation density should not exceed 10^7 cm^{-2} in order to obtain a uniformly high efficiency.

Chichibu *et al*. (*65*) studied the emission mechanisms of GaN and InGaN quantum wells (QWs) by comparing their optical properties as a function of TD density, which was controlled by lateral epitaxial overgrowth technique. The PL intensity was slightly strengthened by reducing TD density from 1×10^{10} cm^{-2} to nearly zero (less than 1×10^6 cm^{-2}). Also, the major PL decay time was independent of the TD density. These results suggested that the emission mechanisms are unaffected by TDs. TDs are considered to simply reduce the net volume of light-emitting area. This effect is less pronounced in InGaN QWs where carriers are effectively localized at certain potential minimum caused by In composition fluctuation in the QWs to form quantized excitons (*24–28*) before being trapped in nonradiative pathways at TDs, which results in a pronounced slow decay time (1 to 40 ns). The depth of these localized energy states with a small In composition fluctuation is enhanced by the large band gap bowing of the InGaN (*66*). Assuming that the lateral spacing of the effective band gap (potential) minimum determines the carrier diffusion length in InGaN, the carrier diffusion length was estimated to be 60 nm (*28*). An absence of change in the Stokes-like shift due to reduction of TD density revealed that the effective band-gap fluctuation in InGaN QWs was not due to a phase separation initiated by TDs (*60*, *61*).

Present progress in InGaN-based LEDs and LDs is described below and takes into consideration the role of the dislocations and the In composition fluctuation in the InGaN layer.

InGaN-Based UV/Blue/Green LEDs

The reason why InGaN-based LEDs are so efficient despite the large number of TDs has not yet been clarified (*45*). However, there are several clues. The high-efficiency LEDs can be obtained only by using InGaN active layer for the LED and LDs. When the active layer of the LEDs is GaN or AlGaN, the efficiency of LEDs is considerably lower (*31*). The PL intensity of band-to-band-emission of GaN layer (*67*) was much weaker than that of InGaN layer (*68*) when they were grown by MOCVD.

III-V nitride films were grown by the two-flow MOCVD method. Details of the two-flow MOCVD are described elsewhere (*3*, *4*). The growth was conducted at atmospheric pressure. Sapphire with (0001) orientation (C face), of 2-inch (5.1-cm) diameter, was used as a substrate. The green LED device structures consist of a 300 Å GaN buffer layer grown at a low temperature (550°C), a 4-μm-thick layer of *n*-type GaN:Si, a 30-Å-thick active layer of undoped $In_{0.45}Ga_{0.55}N$, a 1000-Å-thick layer of *p*-type $Al_{0.2}Ga_{0.8}N$:Mg, and a 0.5-μm-thick layer of *p*-type GaN:Mg. The active region forms a SQW structure consisting of a 30-Å $In_{0.45}Ga_{0.55}N$ well layer sandwiched by 4-μm *n*-type GaN and 1000 Å *p*-type $Al_{0.2}Ga_{0.8}N$ barrier layers (*3*). The In composition of the $In_{0.45}Ga_{0.55}N$ well layer was changed to nearly zero for UV (*31*) and 0.2 for blue LEDs (*33*), respectively. For UV LED, the composition of both *n*- and *p*-type cladding layers was changed to 0.2-μm-thick $Al_{0.2}Ga_{0.8}N$ layers.

Figure 1 shows the cross-sectional TEM images of the LD structure grown on the sapphire substrate. From the cross-sectional TEM, the TD density was estimated to be as high as 1×10^{10} to 10×10^{10} cm^{-2} in the InGaN-based LDs. The InGaN-based LEDs also have the same order of TDs in the InGaN active layer (*45*). In spite of this large number of dislocations, these LEDs have an external quantum efficiency as high as 12%. The conventional LEDs, such as infrared/red AlGaAs and red/yellow AlInGaP LEDs, cannot achieve such high efficiencies when the dislocation density is $>1 \times 10^3$ cm^{-2}. Thus, only InGaN-based LEDs are insensitive to dislocations from the standpoint of efficiency.

The absorption and emission spectra of the LEDs were measured in order to study the InGaN active layer. Photocurrent (PC) spectra of the blue/green InGaN SQW structure LEDs were measured (*69*). Monochromatic light was focused on the epitaxial wafer of each device structure and the PC spectrum was measured. Figure 2A shows the PC spectra and electroluminescence (EL) spectra of the blue and green InGaN SQW LEDs. The EL of the LEDs was measured at a current of 20 mA at RT. The peak wavelengths of the EL of the blue and green InGaN SQW LEDs were 453 nm (2.74 eV) and 520 nm (2.39 eV), respectively, as shown in spectra c and d. Both the PC spectra, a and b, show a strong peak at a wavelength around 360 nm (3.44 eV), which is due to an absorption of the thick GaN layers. In the PC spectra, there are also shoulderlike peaks at 410 nm (3.03 eV) for the blue (a) and 420 nm (2.96 eV) for the green SQW LEDs (b), respectively. These shoulderlike peaks are probably due to the absorption at the $n = 1$ electron heavy hole excitonic transition of the quantum energy level in the InGaN well layer (*24–28*). The Stokes shifts of energy differences between the absorption due to the $n = 1$ quantum energy state and the emission of the blue and green SQW LEDs were 290 and 570 meV, respectively.

When the In-composition ratio of InGaN well layer is increased, fluctuations in In composition increase and an energy tail of the absorption spectra to a lower energy state is formed due to an InGaN-phase separation during the growth (*24–28*). Then, the spectrum width of the PC spectrum of green LEDs (b) becomes broad and

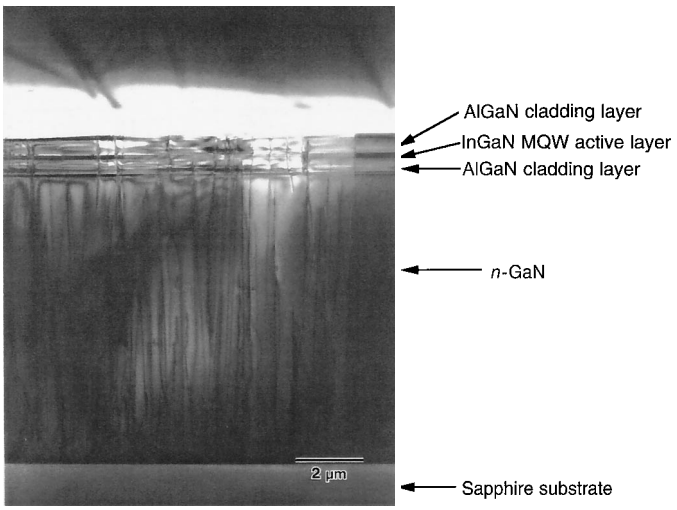

Fig. 1. Cross-sectional transmission electron micrographs (TEM) of the InGaN-MQW/GaN/AlGaN SCH LD grown directly on the sapphire substrate. The LD structure consisted of a 300-Å-thick GaN buffer layer grown at a low temperature of 550°C, a 3-μm-thick layer of *n*-type GaN:Si, a 0.1-μm-thick layer of *n*-type $In_{0.05}Ga_{0.95}N$:Si, a 0.5-μm-thick layer of *n*-type $Al_{0.08}Ga_{0.92}N$:Si, a 0.1-μm-thick layer of *n*-type GaN:Si, an $In_{0.15}Ga_{0.85}N/In_{0.02}Ga_{0.98}N$ MQW structure consisting of three 35-Å-thick Si-doped $In_{0.15}Ga_{0.85}N$ well layers forming a gain medium separated by 70-Å-thick Si-doped $In_{0.02}Ga_{0.98}N$ barrier layers, a 200-Å-thick layer of *p*-type $Al_{0.2}Ga_{0.8}N$:Mg, a 0.1-μm-thick layer of *p*-type GaN:Mg, a 0.5-μm-thick layer of *p*-type $Al_{0.08}Ga_{0.92}N$:Mg, and a 0.3-μm-thick layer of *p*-type GaN:Mg. The 0.1-μm-thick *n*-type and *p*-type GaN layers were light-guiding layers. The 0.5-μm-thick *n*-type and *p*-type $Al_{0.08}Ga_{0.92}N$ layers acted as cladding layers for confinement of the carriers, and the light was emitted from the active region of the InGaN MQW structure.

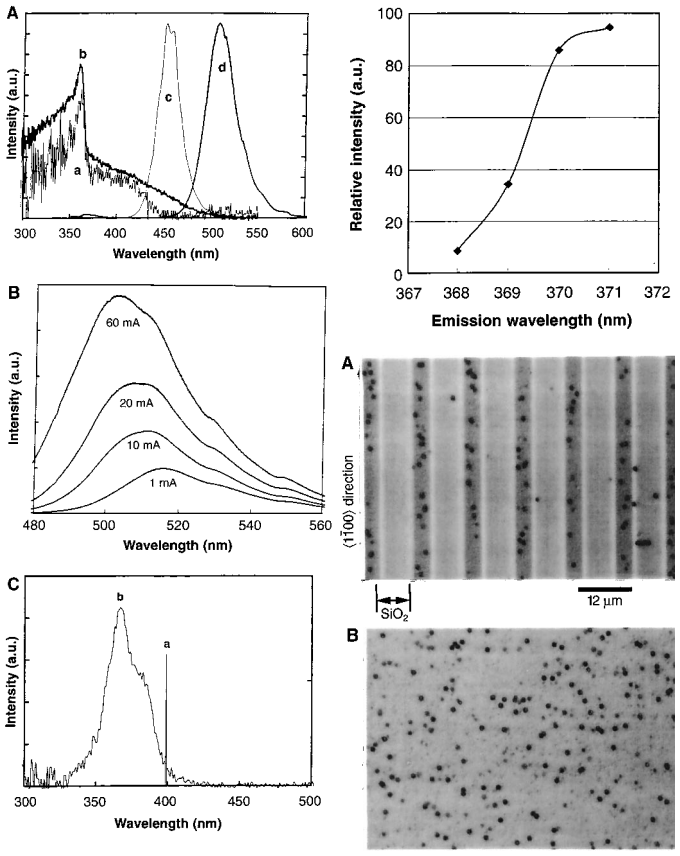

Fig. 2 (left). (**A**) PC and EL spectra of the blue and green InGaN SQW LEDs. (a) PC of the blue, (b) PC of the green, (c) EL of the blue, and (d) EL of the green InGaN SQW LEDs. The EL was observed at a forward current of 20 mA at RT. (**B**) EL of green SQW LEDs with various forward currents. (**C**) (a) Emission and (b) PC spectra of the InGaN-MQW/GaN/AlGaN SCH LD. **Fig. 3 (top right).** The relative output power of the UV LEDs as a function of the emission wavelength with a different In mole fraction in the active layer. **Fig. 4 (bottom right).** Etched surface morphologies of (**A**) the ELOG substrate and (**B**) the 12-μm-thick GaN film grown under the same conditions as the ELOG substrate without the SiO_2 mask patterns. The SiO_2 stripe width and window width of the ELOG substrate were 8 and 4 μm, respectively. The etch pit density was $\sim 2 \times 10^7$ cm^{-2} in the region of the 4-μm-wide stripe window.

the peak wavelength is almost the same for the blue and green LEDs. All of the EL appears at this lower energy tail of the absorption spectra that results from In-composition fluctuation. The EL of blue and green LEDs originates from the carrier recombination at the deep localized energy states with localization energies of 290 and 570 meV, respectively. The depth of these localized energy states with a small In composition fluctuation is also enhanced by the large band gap bowing of the InGaN (*66*). The blue shift of the EL of the green SQW LEDs with increasing forward current (Fig. 2B) is probably due to a band-filling effect of the localized energy states. In the InGaN SQW LEDs, the emission originates from the recombination of localized excitons caused by In composition fluctuation in the InGaN well layer (energy depth is 200 to 600 meV), of which the density of localized energy states is small. Thus, band-filling effects are easily observed.

Because of the low symmetry, the wurtzite system such as GaN-based materials displays pyroelectric and piezoelectric behavior (*25*, *70–72*). The macroscopic polarization in the material comprising the active region of the SQW or MQW gives rise to a net electric field perpendicular to the plane of the well. This field, if strong enough, will induce a spatial separation of the electron and hole wave functions in the well. As the charge density concentrates near the walls of the well, the wave function overlap decreases and the interband recombination rate is reduced [the so-called quantum-confined Stark effect (QCSE)]. The piezoelectric field strength in 1% lattice-mismatched InGaN QW was estimated to be on the order of megavolts per centimeter (*72*), and the Stark shift in 3-nm-thick QW was estimated to be 26 and 274 meV for fields of 1 and 4 MV cm^{-1} (*25*), respectively. In Fig. 2B, the blue shifts of the ELs of the green SQW LEDs with increasing forward current may be explained by the QCSE resulting from piezoelectric fields induced from the lattice mismatch of 1%. However, the EL spectra showed a spectrum broadening and a blueshift with increasing forward currents, which cannot be explained only by the QCSE. Therefore, the blueshift in the EL peak energy may be due to a band filling of the local potential minimum in the potential fluctuation of the InGaN well layer. Also, the higher efficiency of the LEDs with increasing strain in the SQW, due to an increasing In content in the wells, was observed. These phenomena cannot be explained only with the QCSE. The localization effects induced by the composition fluctuations have to overcome these intrinsic limitations due to the piezoelectric field (*24–28*).

The localization induced by the In composition fluctuations seem to be a key role of the high efficiency of the InGaN-based LEDs. When the electrons and holes are injected into the InGaN active layer of the LEDs, these carriers are captured by the localized energy states before they are captured by the nonradiative recombination centers caused by the large number of dislocations. It was reported that the TDs served as a nonradiative recombination center in GaN and InGaN (*50*, *59–62*, *64*). These localized energy states can be formed only in InGaN films during the growth due to a phase separation of the InGaN (*24–28*). Assuming that the lateral spacing of the effective band-gap (potential) minimum determines the carrier diffusion length in InGaN, the diffusion length was estimated to be less than 60 nm from the spatially resolved CL spectrum mapping measurement (*28*). Sugahara *et al.* (*64*) also concluded that the efficiency of light emission is high as long as the minority carrier diffusion length is shorter than the dislocation spacing. Taking these previous results into consideration, the carrier diffusion length determined by the potential fluctuation due to InGaN phase separation must be less than the dislocation spacing in the InGaN layer in order to obtain high-efficiency InGaN-based LEDs.

Figure 3 shows the relative output power as a function of the emission wavelength of the UV LEDs (*31*). The output power of the UV LEDs containing a small amount of In in the active layer, with the emission wavelength of 371 nm, was about 10 times greater than that containing no In with the emission wavelength of 368 nm. Thus, high-power UV LEDs can be obtained only when using the InGaN active layer instead of the GaN active layer. This difference is probably related to the deep localized energy states caused by the In composition fluctuations of the InGaN active layer due to a phase separation during growth (*24–28*). Without In in the active layer, there are no In composition fluctuations that form the deep localized energy state in the InGaN active layer. Thus, the QCSE resulting from the piezoelectric field due to the strain becomes dominant. The efficiency of the UV LEDs therefore becomes extremely low when the active layer is GaN.

The maximum external quantum efficiencies of the LEDs were 7.5% at 371 nm (UV), 11.2% at 468 nm (blue), and 11.6% at 520 nm (green), respectively, which were the highest values reported for the LEDs with those emission wavelengths. The luminous efficiencies of blue and green LEDs were 5 lumens per watt (lm/W) and 30 lm/W, respectively, whereas that of the red AlInGaP LEDs range from 20 to 30 lm/W. The luminous efficiency of the white conventional incandescent bulb lamp is ~20 lm/W (*6*). By combining the blue, green, and red LEDs, we can fabricate white LEDs with a luminous efficiency of 30 lm/W (*6*). The lifetime of the LEDs is longer than 100,000 hours, which is much longer than that of the incandescent bulb lamps. If we could reduce the cost of the LEDs substantially in the future, it would be possible to replace the conventional incandescent bulb lamps with the nitride-based blue, green LEDs and AlInGaP–based red LEDs in order to save consumption of the energy and resources.

InGaN-Based Violet Laser Diodes

The lifetimes of the III-V nitride–based LDs with an active layer of InGaN MQW structure have recently improved to 10,000 hours under conditions of RT-CW operation (*42*). The lifetime of the LDs with an InGaN-MQW/GaN/AlGaN separate confinement heterostructure (SCH) grown on the sapphire substrate was only 300 hours (*73*). The improvement of the lifetime of the LDs was achieved with new substrates with a low TD density (*41–44*). As noted above, the localized states of InGaN layer play a key role in the high efficiency of the LEDs. In the LDs, only InGaN has been used as the active layer because laser oscillation with GaN or AlGaN active layer under current injection has not been achieved. Thus, also for LDs, the InGaN plays an important role in forming the localized states that lead to emission. However, in order to achieve a long lifetime for the LDs, the number of TDs which originated from the interface between GaN and the sapphire substrate had to be reduced.

First, the laser structure was grown directly on sapphire substrate. Therefore, the TD density in the InGaN active layer is as high as 1×10^8 to 1×10^{12} cm^{-2}, as shown in Fig. 1. Figure 2C shows (a) the laser emission and (b) the PC spectrum of this InGaN MQW LD (*69*). By comparing the PC spectrum of the LD in Fig. 2C with those of blue and green InGaN SQW LEDs in Fig. 2A, we determined that the 345-nm (3.59-eV) peak is due to an absorption of $Al_{0.08}Ga_{0.92}N$ cladding layers, the 360-nm (3.44-eV) peak is due to an absorption of GaN guiding layers and $In_{0.02}Ga_{0.98}N$ barrier layers, and the 381-nm (3.25-eV) peak is due to the absorption at the $n = 1$ electron heavy-hole excitonic transition in the $In_{0.15}Ga_{0.85}N$ well layer. The stimulated emission of this LD appeared at 399 nm (3.11 eV) and was positioned at the low-energy tail state of the absorption spectra of the PC spectrum. The Stokes shift of the energy difference between the absorption due to the $n = 1$ QW energy state and the laser emission was 140 meV. This result means that the laser emission also originates from carrier recombination at a deep localized state of $n = 1$ two-dimensional InGaN QW state (*24–28*). Thus, the localized states of InGaN well layer due to the InGaN phase separation play an important role in the high efficiency of LDs despite the large number of TDs. The lifetime of the LDs with this structure of InGaN-MQW/GaN/AlGaN SCH grown directly on the sapphire substrate was only 30 to

300 hours due to a high threshold current density that was probably caused by a large number of TDs (*73*). In order to achieve a long lifetime of 10,000 hours, the dislocation density had to be decreased.

In order to reduce the number of dislocations to lengthen the lifetime of the LD, ELOG substrate was used, which was recently initiated by other groups (*74*, *75*). Also, to grow the thick AlGaN cladding layer with the high Al content required for optical confinement without any cracks, GaN/AlGaN modulation–doped strained-layer superlattices (MD-SLSs) within the range of critical thickness instead of thick AlGaN layers were used as cladding layers (*41–44*). It was difficult to grow a thick AlGaN cladding layer required for optical confinement, due to the formation of cracks during growth in the layers. These cracks are caused by the stress introduced in the AlGaN cladding layers due to lattice mismatch, and by the difference in thermal expansion coefficients between the AlGaN cladding layer and GaN layers. The mechanism of cracking is the relaxation of the strain energy due to the lattice mismatch between AlGaN and GaN during the growth. In the case of a thin AlGaN layer, the elastic strain is not relieved by the formation of cracks and dislocations, and thus the crystal quality of the AlGaN cladding layer improves. The selective growth of GaN was performed on a 2-μm-thick GaN layer grown on a (0001) C-face sapphire substrate. The 0.1-μm-thick silicon dioxide (SiO_2) mask was patterned to form 4-μm-wide stripe windows with a periodicity of 12 μm in the GaN $\langle 1\bar{1}00 \rangle$ direction. After 10-μm-thick GaN was grown on the SiO_2 mask pattern, the coalescence of the selectively grown GaN made it possible to obtain a flat GaN surface over the entire substrate. We call this coalesced GaN epitaxially laterally overgrown GaN, or ELOG. Figure 4A shows the etched surface morphology of the ELOG substrate, and Fig. 4B shows that of the 12-μm-thick GaN film grown under the same conditions as the ELOG substrate without the SiO_2 mask patterns for comparison (*41–44*). The etching of the GaN was performed by reactive ion etching with Cl_2 plasma (*3*). The etching depth was as great as 2 μm in order to reveal the etch pit clearly. Many hexagonal etch pits with the number of 1×10^8 cm^{-2} were observed over the entire region of the GaN film grown directly on the sapphire substrate, as shown in Fig. 4B. On the ELOG substrate, a small number of etch pits were observed on the 4-μm-wide stripe window, as shown in Fig. 4A. The etch pit density was about 2×10^7 cm^{-2} in the region of the 4-μm-wide stripe window. However, the etch pit density was almost zero in the region of the 8-μm-wide SiO_2 stripe.

Figure 5 shows cross-sectional TEM image of the ELOG substrate. TDs, originating from the GaN/sapphire interface, propagate to the regrown GaN layer within the window regions of the mask, as shown in Fig. 5. It is important to note that the TDs extend only to just above the window areas. In contrast, there were no observable TDs in the overgrown layer. However, a few short edge-on dislocation segments parallel to the interface plane were observed in the GaN layer on the SiO_2 mask area. These dislocations were parallel to the (0001) plane via the extension of the vertical threading dislocations after a 90° bend in the regrown region. These dislocations did not subsequently propagate to the surface of the overgrown GaN layers. We examined the defect density by plan-view TEM observation of the surface of the ELOG substrates. The number of dislocations on the SiO_2 mask area was almost zero within the area of 10 μm by 10 μm, and that on the window area was approximately 1×10^7 cm^{-2}. As the dislocation density of conventional GaN was of the order of 1×10^{10} cm^{-2}, the number of the TDs was reduced considerably when the ELOG substrate was used. These results are almost identical to those obtained through the measurements of etch pit density in Fig. 4 and to the previous work (*74*, *75*).

After obtaining the 10-μm-thick ELOG substrate, the same laser structure was grown on the ELOG substrate. The structure of the ridge-geometry InGaN MQW LD was almost the same as that described previously (*3*). The ridge-geometry LDs were formed on the GaN layers above the SiO_2 region without dislocations and the window region with a high dislocation density. Voltage-current (*V-I*) characteristics and the light output power per coated facet of

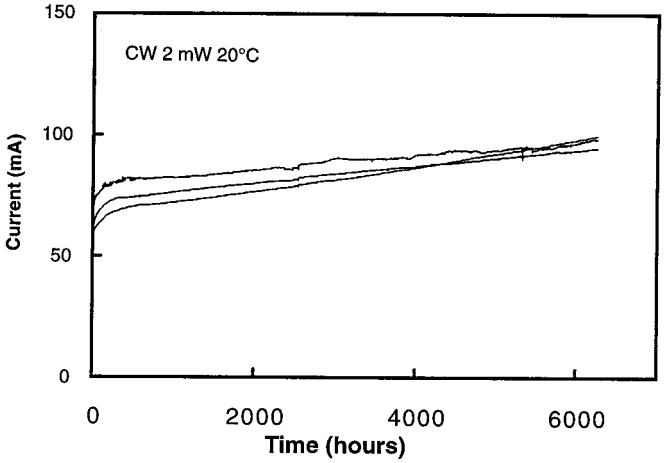

Fig. 6. Operating current as a function of time under a constant output power of 2 mW per facet controlled with an autopower controller. The LDs with MD-SLS cladding layers grown on the ELOG substrate were operated under dc at RT.

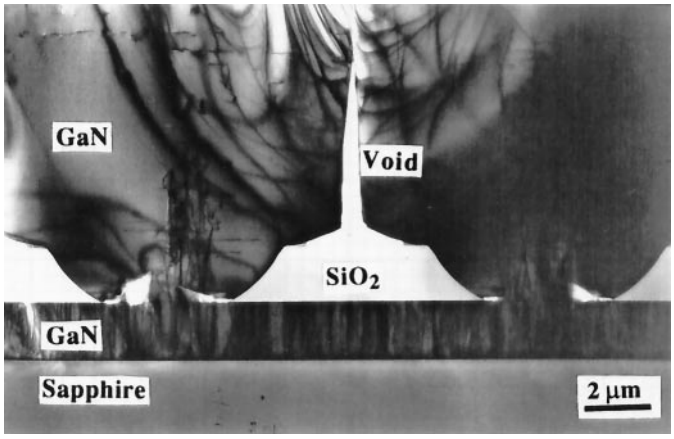

Fig. 5. Cross-sectional TEM micrograph of the laterally overgrown GaN layer on a SiO_2 mask and window area.

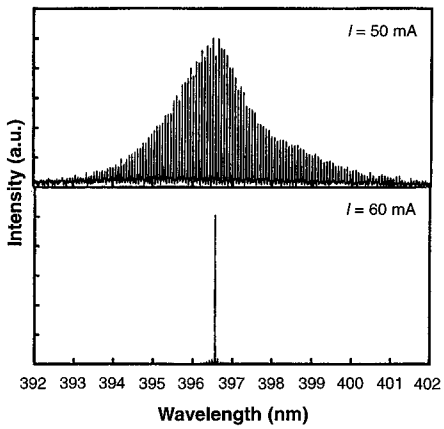

Fig. 7. Laser emission spectra measured under RT CW operation with currents of 50 and 60 mA.

the LD with a cavity length of 450 μm and a ridge width of 4 μm as a function of the forward dc current (*L-I*) at RT were measured (*41*, *42*). When the LD was formed on the GaN layer above the SiO_2 mask region without any dislocations, the threshold current was 53 mA, which corresponded to a threshold current density of 3 kA cm^{-2}. The LD formed on the window region with the high dislocation density had a threshold current density of 6 to 9 kA cm^{-2}, which was much greater than that of the LD formed on the SiO_2 mask. The higher threshold current density is probably caused by the large number of TD density of 1×10^7 cm^{-2} at the window region. It was reported that the TD served as a diffusion pathway of metals, and did as a leakage current pathway in InGaN and GaN (*57*, *58*). Thus, it is possible that a leakage current due to a large number of TDs caused the high threshold current density on the window region. Further studies are required to determine the reasons for the high threshold current density caused by TDs.

Figure 6 shows the results of a lifetime test for CW-operated LDs formed on the GaN layer above the SiO_2 mask region carried out at 20°C, in which the operating current is shown as a function of time under a constant output power of 2 mW per facet controlled with an autopower controller. The LDs survived 6000 hours of operation. The lifetime of some of the LDs was estimated to be longer than 10,000 hours from the degradation speed. The degradation speed was defined as the derivative of dI/dt (mA/100 hours), where I is the operating current of the LDs and t is the time. Using this degradation speed, the estimated lifetime was determined as the time when the operating current became twice the initial operating current of the LDs. The lifetimes of LDs formed on the window region were 1000 to 2000 hours due to the high threshold current density of 6 to 9 kA cm^{-2}.

The emission spectra of the LDs were measured under RT CW operation at currents of 50 and 60 mA (Fig. 7). An optical spectrum analyzer (ADVANTEST Q8347), which makes use of the Fourier-transform spectroscopy method by means of a Michelson interferometer, was used to measure the spectra of the LDs with a resolution of 0.001 nm. At a current of 50 mA, longitudinal modes with a mode separation of 0.04 nm due to the cavity were observed. At a current of 60 mA, a single-mode emission was observed at an emission wavelength of 396.6 nm.

Conclusions

UV/blue/green/amber InGaN-based LEDs were obtained with an InGaN active layer instead of a GaN active layer. The localized energy states caused by In composition fluctuation in the InGaN active layer are related to the high efficiency of the InGaN-based LEDs and LDs. The QCSE resulting from the piezoelectric field due to the strain seems not to be dominant by the In composition fluctuation. However, the QCSE must be included to explain the emission mechanism in detail because the strong piezoelectric field must exist in the InGaN well layer due to a large lattice mismatch and a coherent growth between InGaN and GaN layers. A large Stokes shift and a long decay time of the spontaneous emission may be related to the QCSE. Further studies are required on this QCSE. InGaN MQW LDs with MD-SLS cladding layers fabricated on the ELOG substrate were demonstrated to have an estimated lifetime of more than 10,000 hours under conditions of RT CW operation. The emission wavelength of the LDs is around 400 nm, which is suitable for the next generation of the 15-Gbyte DVDs. The TD increased the threshold current density of the LDs. Considering this behavior of TDs for the LD, free-standing GaN substrates, which are made by growing the thick ELOG (200 μm) and removing the sapphire, would be a promising substrate because of the lack of a large size bulk GaN substrate (*44*).

References

1. S. Yoshida, S. Misawa, S. Gonda, *Appl. Phys. Lett.* **42**, 427 (1983).
2. H. Amano, N. Sawaki, I. Akasaki, T. Toyoda, *ibid.* **48**, 353 (1986).
3. Reviewed by S. Nakamura and G. Fasol, *The Blue Laser Diode* (Springer-Verlag, Heidelberg, ed. 1, 1997).
4. S. Nakamura, *Jpn. J. Appl. Phys.* **30**, L1705 (1991).
5. S. Strite and H. Morkoç, *J. Vacuum Sci Technol.* B**10**, 1237 (1992).
6. F. A. Ponce and D. P. Bour, *Nature* **386**, 351 (1997).
7. J. I. Pankove, E. A. Miller, J. E. Berkeyheiser, *RCA Rev.* **32**, 383 (1971).
8. J. I. Pankove, M. T. Duffy, E. A. Miller, J. E. Berkeyheiser, *J. Luminescence* **8**, 89 (1973).
9. H. P. Maruska, W. C. Rhines, D. A. Stevenson, *Mat. Res. Bull.* **7**, 777 (1972).
10. O. Lagerstedt and B. Monemar, *J. Appl. Phys.* **45**, 2266 (1974).
11. H. Amano, M. Kito, K. Hiramatsu, I. Akasaki, *Jpn. J. Appl. Phys.* **28**, L2112 (1989).
12. S. Nakamura, T. Mukai, M. Senoh N. Iwasa, *ibid.* **31**, L139 (1992).
13. S. Nakamura, N. Iwasa, M. Senoh T. Mukai, *ibid.*, p. 1258.
14. C. Wang and R. F. Davis, *Appl. Phys. Lett.* **63**, 990 (1993).
15. M. Rubin, N. Newman, J. S. Chan, T. C. Fu, J. T. Ross, *ibid.* **64**, 64 (1994).
16. M. S. Brandt, N. M. Johnson, R. J. Molnar, R. Singh, T. D. Moustakas, *ibid.*, p. 2264.
17. J. M. Zavada, R. G. Wilson, C. R. Abernathy, S. J. Pearton, *ibid.*, p. 2724.
18. J. Neugebauer and C. Van De Walle, *Phys. Rev.* B**50**, 8067 (1994).
19. T. Nagatomo, T. Kuboyama, H. Minamino, O. Omoto, *Jpn. J. Appl. Phys.* **28**, L1334 (1989).
20. T. Matsuoka, H. Tanaka, T. Sasaki, A. Katsui, *Inst. Phys. Conf. Ser.* **106**, 141 (1990).
21. T. Matsuoka, *J. Cryst. Growth* **124**, 433 (1992).
22. S. Nakamura and T. Mukai, *Jpn. J. Appl. Phys.* **31**, L1457 (1992).
23. S. Nakamura, T. Mukai, M. Senoh, S. Nagahama N. Iwasa, *J. Appl. Phys.* **74**, 3911 (1993).
24. S. Chichibu, T. Azuhata, T. Sota, S. Nakamura, *Appl. Phys. Lett.* **69**, 4188 (1996).
25. ———, *ibid.* **70**, 2822 (1997).
26. Y. Narukawa, Y. Kawakami, Sz. Fujita, Sg. Fujita, S. Nakamura, *Phys. Rev.* **B55**, 1938R (1997).
27. Y. Narukawa *et al.*, *Appl. Phys. Lett.* **70**, 981 (1997).
28. S. Chichibu, K. Wada, S. Nakamura, *ibid.* **71**, 2346 (1997).
29. S. Nakamura, T. Mukai M. Senoh, *ibid.* **64**, 1687 (1994).
30. S. Nakamura *et al.*, *Jpn. J. Appl. Phys.* **34**, L1332 (1995).
31. T. Mukai, D. Morita, S. Nakamura, *J. Crystal Growth* **189/190**, 778 (1998).
32. T. Mukai, H. Narimatsu S. Nakamura, *Jpn. J. Appl. Phys.* **37**, L479 (1998).
33. S. Nakamura *et al.*, *ibid.* **35**, L74 (1996).
34. K. Itaya *et al.*, *ibid.*, p. L1315.
35. G. E. Bulman *et al.*, *Electron. Lett.* **33**, 1556 (1997).
36. M. P. Mack *et al.*, *MRS Internet J. Nitride Semicond. Res.* **2**, 41 (1997). Available at http://nsr.mij.mrs.org/2/41/.
37. A. Kuramata *et al.*, *Jpn J. Appl. Phys.* **36**, L1130 (1997).
38. F. Nakamura *et al.*, in (*31*), p. LN-8.
39. M. Kneissl *et al.*, *Appl. Phys. Lett.* **72**, 1539 (1998).
40. H. Katoh *et al.*, *Jpn. J. Appl. Phys.* **37**, L 444 (1998).
41. S. Nakamura *et al.*, *Appl. Phys. Lett.* **72**, 211 (1998).
42. ———, *Jpn. J. Appl. Phys.* **36**, L1568 (1997).
43. ———, *ibid.* **37**, L627 (1998).
44. ———, *ibid.*, p. L309.
45. S. D. Lester, F. A. Ponce, M. G. Craford, D. A. Steigerwald, *Appl. Phys. Lett.* **66**, 1249 (1995).
46. D. Kapolnek *et al.*, *ibid.* **67**, 1541 (1995).
47. X. H. Wu *et al.*, *Jpn. J. Appl. Phys.* **35**, L1648 (1996).
48. B. Heying *et al.*, *Appl. Phys. Lett.* **68**, 643 (1996).
49. B. Garni *et al.*, *ibid.*, p. 1380.
50. S. J. Rosner *et al.*, *ibid.* **70**, 420 (1997).
51. N. G. Weimann and L. F. Eastman, *J. Appl. Phys.* **83**, 3656 (1998).
52. P. J. Hansen *et al.*, *Appl. Phys. Lett.* **72**, 2247, (1998).
53. W. Qian *et al.*, *ibid.* **67**, 2284 (1995).
54. X. H. Wu *et al.*, *J. Appl. Phys.* **80**, 3228 (1996).
55. E. J. Tarsa *et al.*, *ibid.* **82**, 5472 (1997).
56. F. A. Ponce, D. P. Bour, W. Gotz, P. J. Wright, *Appl. Phys. Lett.* **68**, 57 (1996).
57. C. Sasaoka *et al.*, *J. Crystal Growth* **189/190**, 61 (1998).
58. A. Osinsky *et al.*, *Appl. Phys. Lett.* **71**, 2334 (1997).
59. X. H. Wu *et al.*, *ibid.* **72**, 692 (1998).
60. H. Sato, T. Sugahara, Y. Naoi, S. Sakai, *Jpn. J. Appl. Phys.* **37**, 2013 (1998).
61. S. Keller, U. K. Mishra, S. P. Denbaars, W. Seifert, *ibid.*, p. L431.
62. Y. Chen *et al.*, *Appl. Phys. Lett.* **72**, 710 (1998).
63. P. A. Crowell, D. K. Young, S. Keller, E. L. Hu, D. D. Awschalom, *ibid.*, p. 927.
64. T. Sugahara *et al.*, *Jpn. J. Appl. Phys.* **37**, L398 (1998).
65. S Chichibu *et al.*, in preparation.
66. M. D. McCluskey, C. G. Van de Walle, C. P. Master, L. T. Romano, N. M. Johnson, *Appl. Phys. Lett.* **72**, 2725 (1998).
67. S. Nakamura, T. Mukai, M. Senoh, *Jpn. J. Appl. Phys.* **31**, 2883 (1992).
68. ———, *ibid.* **32**, L16 (1993).
69. S. Nakamura, *IEEE J. Selective Top. Quantum Electron.* **3**, 712 (1997).
70. D. L. Smith and C. Mailhiot, *Phys. Rev. Lett.* **58**, 1264 (1987).
71. M. B. Nardelli, K. Rapcewicz, J. Bernholc, *Appl. Phys. Lett.* **71**, 3135 (1997).
72. T. Takeuchi *et al.*, *Jpn. J. Appl. Phys.* **36**, L177 (1997).
73. S. Nakamura *et al.*, *ibid.*, p. L1059.
74. A. Sakai, H. Sunakawa, A. Usui, *Appl. Phys. Lett.* **71**, 2259 (1997).
75. T. S. Zheleva, O. H. Nam, M. D. Bremser, R. F. Davis, *ibid.*, p. 2472.

Effects of Random Perturbations in Plastic Optical Fibers

A. F. Garito, J. Wang, R. Gao

REVIEW

The most important feature of an optical fiber waveguide is its bandwidth, which defines its information-carrying capacity. A major limitation on the bandwidth of multimode glass and plastic optical fibers is modal dispersion, in which different optical modes propagate at different velocities and the dispersion grows linearly with length. However, in plastic optical fibers, experimental and theoretical results indicate that the modes are not independent but are highly coupled, which leads to a characteristic square-root length dependence and an unanticipated large enhancement of the bandwidth to gigahertz levels. The ever increasing demands for low-cost, high-bandwidth communications media for voice, video, and data transmission in short- and medium-distance applications are generating a new assessment of multimode optical fibers to serve as high-speed fiber links.

Optical communication systems based on glass optical fibers (GOFs) allow communication signals to be transmitted not only over long distances with low attenuation but also at extremely high data rates, or bandwidth capacity. This capability arises from the propagation of a single optical signal mode in the low-loss windows of glass located at the near-infrared wavelengths of 0.85, 1.3, and 1.55 μm. Since the introduction of erbium-doped fiber amplifier (EDFA), the last decade has witnessed the emergence of single-mode GOF as the standard data transmission medium for wide area networks (WANs), especially in terrestrial and transoceanic communication backbones. In addition, the bandwidth performance of single-mode GOF has been vastly enhanced by the development of dense wavelength division multiplexing (DWDM), which can couple up to 40 channels of different wavelengths of light (colors) into a single fiber, with each channel carrying gigabits of data per second. Moreover, in a recent demonstration by Lucent Technologies, signal transmission of 1 terabit (10^{12} bits) per second was achieved over a single fiber on a 100-channel DWDM system. Enabled by these and other technologies, the bandwidth capacities of the communication networks are increasing at rates of as much as an order of magnitude per year.

The success of the single-mode GOF in long-haul communication backbones has given rise to the concept of optical networking, which is a central theme currently driving research and development activities in the field of photonics. The main objective is to integrate voice, video, and data streams over all-optical systems as communication signals make their way from WANs down to smaller local area networks (LANs), and eventually to the end user by fiber to the desktop (FTTD). Examples are the recent explosion of the Internet and use of the World Wide Web, which are demanding vastly higher bandwidth performance in short- and medium-distance applications. However, the single-mode GOF core is typically only a few micrometers in diameter. Yet as the optical network nears the end user starting at the LAN stage, the system is characterized by numerous connections, splices, and couplings that make the use of thin single-mode GOF impractical. Current solutions depend on multimode GOF with a larger core diameter (typically 50 or 62.5 μm) to ease these fiber connection and systems installation issues. However, the increased fiber diameter is accompanied by an increase in the number of optical signal modes to many tens of thousands and consequent optical pulse broadening. The unwanted pulse broadening is due to modal dispersion, in which different modes (light paths) within the fiber carry components of the signals at different velocities, ultimately results in pulse overlap and a garbled communications signal. Additional pulse broadening contributions from wavelength-dependent dispersion (material dispersion) and intramodal (waveguide) dispersion due to the wavelength dependence of the modal group velocity also occur, but to a lesser extent than modal dispersion (*1*). To overcome and compensate for modal dispersion, the refractive index of the fiber core is graded parabola-like from a high index at the fiber core center to a low index in the outer core region, so that the high-order and low-order modes inside the fiber travel at the same group velocity (*2, 3*).

GOF is brittle and fragile at large core diameters; hence, plastic optical fiber (POF) (Fig. 1A) is being seriously considered as a high-bandwidth fiber link for certain short-distance applications because of its ductility and large core diameter (1 mm). Similar to its GOF counterpart, the bandwidth performance of multimode POF is limited by modal dispersion of the signal pulses. This problem can be alleviated by forming graded-index (GI) POF that has a parabola-like index profile.

In this article, we discuss a different approach to overcoming dispersion that also leads to improvements in the bandwidth of POFs. Rather than trying to force all of the modes to travel at the same velocity, we studied the approach of mode coupling, or mode mixing (*4–6*). Recent experiments on POFs in our research group have revealed unanticipated large enhanced bandwidths due to random index perturbations and mode coupling (*7, 8*), which is our main topic here.

Modal dispersion in the optical fiber waveguide is reduced through mode coupling by allowing the energy packets of the input signal pulse to occupy different modes at different times as they are propagating down the waveguide. These conditions can occur by way of random perturbations along the propagation direction of the fiber waveguide. The perturbations induce coupling between the different modes and cause the energy packets to randomly switch modes back and forth, much as automobiles usually interchange lanes during natural traffic flow. In the presence of mode coupling, the modes are no longer independent, and the energy packets in each mode now travel at an averaged group velocity to arrive essentially at the same time at the output end of the waveguide. As a result, the pulse broadening of the output pulse is markedly reduced. With mode coupling, pulse broadening varies only as a characteristic square-root function of the fiber length, as opposed to following a linear dependence (*4–6*). A beautiful example of this characteristic square-root length dependence of pulse broadening is based on a simple random walk model of pulse propagation down a one-dimensional waveguide.

Mode Coupling Models

A light pulse propagating in the fiber consists of many energy packets that are distributed over all guided modes. After a certain waveguide length, or coupling length L_c, has been traversed, the relative energy packet population in each mode no longer changes with propagation

The authors are in the Department of Physics and Astronomy, University of Pennsylvania, Philadelphia, PA 19104, USA.